

Article

Effective Removal of Lead Ions from Aqueous Solution Using Nano Illite/Smectite Clay: Isotherm, Kinetic, and Thermodynamic Modeling of Adsorption

Juan Yin ^{1,2}, Chaobing Deng ^{1,3,*}, Zhen Yu ⁴, Xiaofei Wang ³ and Guiping Xu ^{1,3}

¹ College of Light industry and Food Engineering, Guangxi University, Nanning 530004, China; yinjuan101@163.com (J.Y.); xuguiping@126.com (G.X.)

² Department of Management Science and Engineering, Guangxi University of Finance and Economics, Nanning 530003, China

³ Guangxi Zhuang Autonomous Region Environmental Monitoring Center, Nanning 530028, China; wangxiaofei26@163.com

⁴ College of Resources, Environment and Materials, Guangxi University, Nanning 530004, China; yz2465@hotmail.com

* Correspondence: dcb715@sina.com; Tel.: +86-771-532-5805

Received: 14 January 2018; Accepted: 13 February 2018; Published: 16 February 2018

Abstract: Illite-smectite clay is a new mixed mineral of illite and montmorillonite. The ability of nano illite/smectite clay to remove Pb(II) from slightly polluted aqueous solutions has been investigated. The effects of pH, contact time, initial concentration of Pb(II), nano illite/smectite clay dosage, and temperature on the adsorption process were studied. The nano illite/smectite clay was characterized by X-Ray Diffraction (XRD), Fourier transform infrared spectrometry (FTIR), and Scanning electron microscopy (SEM). The results showed that Pb(II) was adsorbed efficiently by nano illite/smectite clay in aqueous solution. The pseudo-second-order kinetic model best described the kinetic of the adsorption, and the adsorption capacity of nano illite/smectite (I-S_m) clay was found to be 256.41 $\mu\text{g}\cdot\text{g}^{-1}$ for Pb(II). The adsorption patterns followed the Langmuir isotherm model. Thermodynamic parameters, including the Gibbs free energy (ΔG), enthalpy (ΔH), and entropy (ΔS) changes, indicated that the present adsorption process was feasible, spontaneous, and endothermic in the temperature range of 298–333 K.

Keywords: Pb(II); nano illite/smectite clay; adsorption kinetics; adsorption thermodynamic

1. Introduction

Water is a source of life. In recent years, a large number of studies have indicated that the water, especially of rivers, in urban areas has been seriously contaminated by heavy metals [1–3]. Because heavy metals are not readily degradable in nature and accumulate in animals as well as human bodies, people who drink water or eat food containing heavy metals for a long time are susceptible to disease. Therefore, heavy metal contamination in the water environment has attracted great concern owing to its environmental toxicity and persistence.

Lead is a widely distributed and accumulative pollutant, and is the third-most common toxic element in the heavy metal toxicity list. It is also one of the 10 chemicals that the World Health Organization (WHO) has set out as a cause for significant public health concerns. Once the lead in the environment through various ways enters the human body and accumulates, the nerve, digestive, immune, and reproductive systems will be compromised and the health of human beings will be threatened, especially that of children [4,5]. The permissible limit for lead in potable water is 0.01 $\text{mg}\cdot\text{L}^{-1}$ [6]. The removal of Pb(II) has become a great concern globally due to these toxic effects of Pb(II) on living beings. In the past few years, various techniques have been used, such as chemical

precipitation, membrane filtration, ion exchange, and biological treatment, for lead removal [7–10]. Among these methods, adsorption has the advantages of being easy to perform and having a low cost and high efficiency. Thus, it has been used commonly in the heavy metal pollution treatment of water [11].

Clay as an adsorbent is widely used for the removal of heavy metals and has great applicability due to its being economical and having an environment-friendly nature, a high adsorption capacity, and a wide pH range [12,13]. In recent years, many kinds of clay, i.e., bentonite, kaolin, and montmorillonite, have been reported for the removal of high-concentration heavy metals from water [13–17]. Illite-smectite (I-S_m) clay is a new mixed mineral of illite and montmorillonite, and a transition mineral from montmorillonite to illite, belonging to the typical 2:1-type layered silicate mineral. In 2014, nearly 30 billion tons of I-S_m mineral was discovered in Shangsi County, Guangxi. Because I-S_m mineral has the characteristics of high purity, fine particles, and a large surface area, I-S_m has been studied for use as a rubber modifier [18] and as an adsorbent to remove high concentrations of heavy metals from aqueous solution [19,20]. Only a few studies have focused on the adsorption of low concentrations of heavy metals in contaminated water using I-S_m.

In this study, the I-S_m mineral was first made nano-size, then nano I-S_m was used to adsorb Pb(II) in a solution close to that of real polluted water. The effects of various analytical conditions, such as initial pH of the solution, contact time, and initial adsorbate and adsorbent concentration, were evaluated in detail on the removal performance of nano I-S_m. Isotherm, kinetic, and thermodynamic modeling of the adsorption process was analyzed.

2. Materials and Methods

2.1. Preparation of Nano I-S_m

I-S_m mineral was provided by Sino-nanotech Holdings Co., Ltd. (Shangsi, Guangxi, China). The main steps of nano I-S_m preparation included crushing, soaking, dispersing, sieving and purification, and ultrafine grinding [18,21]. In detail, the preparation was as follows. Firstly, I-S_m mineral was crushed into small pieces ($d < 2$ cm) and then soaked in a certain amount of water (the water-to-clay ratio was 9:11) for about 10 h. Secondly, the soaked I-S_m mud was dispersed for 30 min with a mixer beater and then passed through a 100-mesh and 325-mesh vibrating screen to obtain the primary nano I-S_m slurry ($d < 45$ μm). Thirdly, the slurry was ground by a high energy density medium stirring mill (FPML OML-H/V, Buhler Group Co., Uzwil, Switzerland) for 2 h. Finally, the slurry was dried by azeotropic distillation and then dispersed by high-speed mill.

2.2. Characterization of Nano I-S_m

The Fourier transform infrared (FT-IR) spectra of nano I-S_m were recorded with the Fourier transform infrared spectrophotometer (Nicolet 380, Thermo Fisher, Waltham, MA, USA). The X-ray diffraction (XRD) analysis was determined using a MiniFlex X-ray diffractometer (Miniflex 600, Rigaku, Tokyo, Japan), and the scanning regions of the diffraction were 5–80° on the 2θ angle. The morphology of nano I-S_m was analyzed by a scanning electron microscope (SEM) (ProX, Phenom World, Shanghai, China), The Brunauer-Emmett-Teller (BET) surface area and pore properties of nano I-S_m were determined via N₂ adsorption–desorption isotherms using a Micromeritics analyzer (ASAP 2460, Micromeritics, Norcross, GA, USA). The cation exchange capacity (CEC) of nano I-S_m was determined by the ammonium acetate method [22]. The slurry's pH was determined by soaking 1 g of nano I-S_m in 50 mL distilled water, stirring the solution for 24 h, filtering it, and then measuring the final pH [23].

2.3. Batch Adsorption Experiments

Stock solutions of Pb(II) were prepared by dissolving appropriate amounts of (CH₃COO)₂Pb·3H₂O in distilled water. Batch adsorption experiments were carried out in a series of centrifuge tubes by mixing a constant amount of nano I-S_m with 40 mL of the aqueous solution of Pb(II) at varying concentration

and different temperatures. Then, the centrifuge tubes were put in a shaker incubator at 150 rpm for a certain time interval, the nano I-S_m was separated from the aqueous solutions by centrifugation at 3000 rpm for 5 min (TDZ5-WS, Cence, Changsha, China), and the supernatant was filtered through a 0.45 µm filter membrane. Pb(II) concentration in the solutions was measured by inductively coupled plasma mass spectrometry (7700 e, Agilent Technologies, Santa Clara, CA, USA).

The adsorption capacity of Pb(II) on nano I-S_m in the batch test was calculated using Equations (1) and (2).

$$R_{ratio} = \frac{C_0 - C_{eq}}{C_0} \times 100\% \quad (1)$$

$$Q_e = \frac{(C_0 - C_{eq})V}{m} \quad (2)$$

where R_{ratio} is the Pb(II) removal rate; Q_e is the equilibrium capacity of lead on the nano I-S_m, mg·g⁻¹; C_0 is the initial concentration of the Pb(II) solution, mg·L⁻¹; C_{eq} is the equilibrium concentration of the Pb(II) solution, mg·L⁻¹; V is the solution volume, L; and m is the mass of nano I-S_m, g. All assays were carried out in triplicate and only mean values are presented.

The effects of process variables, including pH of the solution, initial concentration of Pb(II), contact time, adsorbent dosage, and temperature, on the adsorption were studied. The pH of the solution at the start of the experiments was adjusted with 0.1 mg·L⁻¹ HCl or 0.1 mg·L⁻¹ NaOH. Adsorption isotherms studies were conducted at 298, 308, 313, 323, and 333 K, whereby 0.1 g of nano I-S_m was kept in contact with 40 mL of Pb(II) solution of varying concentrations (0.25, 0.50, 1.50, 2.50, 3.50, and 5 mg·L⁻¹) at pH 5. The kinetic experiments were performed using a Pb(II) concentration of 1 mg·L⁻¹ with 0.1 g nano I-S_m at different time intervals (5, 10, 20, 30, and 60 min) at pH 5.

2.4. Theoretical Model

2.4.1. Adsorption Kinetics Model

The equations of the pseudo-first-order [24] and the pseudo-second-order kinetic model [25] were used to fit experiment data obtained from the batch experiments. The formulas of the pseudo-first-order and the pseudo-second-order kinetic model are expressed as Equations (3) and (4), respectively.

$$\ln(Q_e - Q_t) = \ln Q_e - k_1 t \quad (3)$$

$$\frac{t}{Q_t} = \frac{1}{k_2 Q_e^2} + \frac{1}{Q_e} t \quad (4)$$

where Q_t is the amount of Pb(II) adsorbed at time t , mg·g⁻¹, k_1 is the pseudo-first-order rate constant adsorption rate, min⁻¹; and k_2 is the adsorption rate constant in the pseudo-second-order kinetic rate constant, g·µg⁻¹·min⁻¹.

2.4.2. Adsorption Equilibrium

The isotherm models of Langmuir [26] and Freundlich [27] were tested to analyze the equilibrium data. The Langmuir isotherm model and Freundlich isotherm model equations are expressed by Equations (5) and (6).

$$\frac{C_{eq}}{Q_e} = \frac{1}{Q_{max}} C_{eq} + \frac{1}{Q_{max} K_L} \quad (5)$$

$$\ln Q_e = \ln K_f + \frac{1}{n} \ln C_{eq} \quad (6)$$

where Q_{max} is the monolayer capacity of nano I-S_m, mg·g⁻¹; K_L is the Langmuir constant, L·µg⁻¹; K_f is the Freundlich constant, µg·g⁻¹; and n is the heterogeneity.

2.4.3. Adsorption Thermodynamics

The thermodynamic parameters can be determined using the equilibrium constant and temperature [28,29]. The change in the Gibbs free energy (ΔG), enthalpy (ΔH), and entropy (ΔS) in the adsorption process was calculated using Equations (7) and (8).

$$\Delta G = -RT \ln K_d \quad (7)$$

$$\ln K_d = \frac{\Delta S}{R} - \frac{\Delta H}{RT} \quad (8)$$

where R is the universal gas constant, $8.314 \text{ J} \cdot \text{mol}^{-1} \cdot \text{K}^{-1}$; T is the absolute temperature, K; and K_d is the distribution coefficient of nano I-S_m, $K_d = Q_e / C_{eq}$.

3. Results

3.1. Characterization of Nano I-S_m

The chemical composition and physicochemical properties of nano I-S_m are presented in Table 1. The XRD patterns of nano I-S_m are given in Figure 1 A. Nano I-S_m is mainly composed of quartz, mixed-layer illite/smectite, illite, and kaolinite, and the characteristic diffraction peak of nano I-S_m was observed between 5 and 10° (2θ) [30]. Furthermore, an FT-IR analysis was applied to identify the functional groups on the nano I-S_m sample's surface. The FT-IR spectra of the nano I-S_m sample are shown in Figure 1B. The absorption bands at 3698.96 and 3620.60 cm^{-1} represent the inner surface OH stretching vibration, while the absorption band at 3423.76 cm^{-1} represents the outer surface OH stretching vibration. These OH groups function as an active site for the binding of positively charged cations. The absorption band at 1629.97 cm^{-1} represents the OH bending of water retained in the silica matrix [23]. The absorption bands at 1031.99 and 470.19 cm^{-1} represent the Si–O–Si stretching vibration [31]. The absorption band at 912.4 cm^{-1} represents the Al–OH bending vibrations [29], while those at 798.04 and 694.4 cm^{-1} represent the Si–O stretching vibration [23].

Table 1. Chemical composition and physicochemical properties of nano illite-smectite (I-S_m) clay.

Parameter	Value
SiO ₂ (wt %)	64.29
Al ₂ O ₃ (wt %)	20.38
Fe ₂ O ₃ (wt %)	2.95
K ₂ O (wt %)	2.74
MgO (wt %)	1.82
TiO ₂ (wt %)	0.82
Na ₂ O (wt %)	0.19
Loss of ignition (wt %)	6.46
BET surface area ($\text{m}^2 \cdot \text{g}^{-1}$)	39.46
Micropore area ($\text{m}^2 \cdot \text{g}^{-1}$)	10.46
External surface area ($\text{m}^2 \cdot \text{g}^{-1}$)	28.99
Total pore volume ($\text{cm}^3 \cdot \text{g}^{-1}$)	0.011
Micropore volume ($\text{cm}^3 \cdot \text{g}^{-1}$)	0.0055
Adsorption average pore diameter (4 V/A by BET)	1.07
CEC (meg/100 g)	2.11
Slurry pH	6.75

CEC: cation exchange capacity. BET: Brunauer-Emmett-Teller.

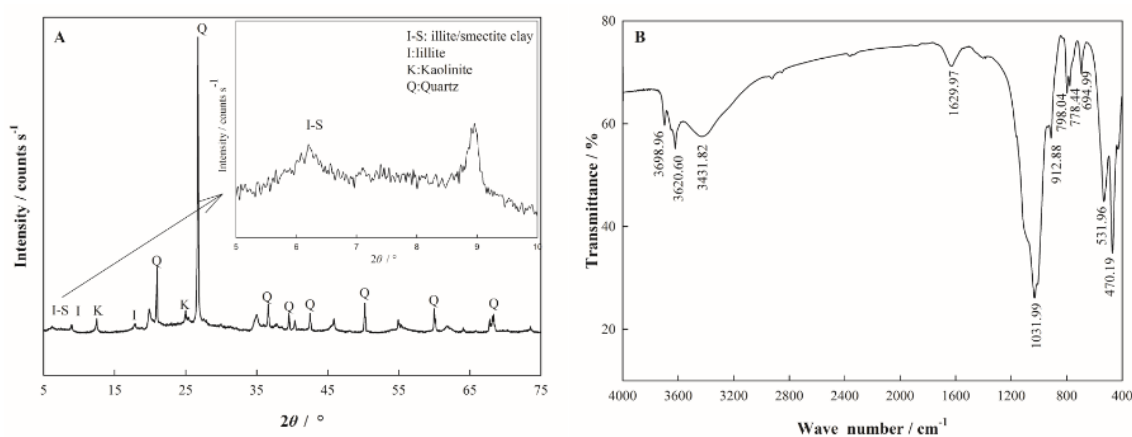


Figure 1. XRD spectra (A) and FT-IR spectrum (B) of nano I-S_m.

SEM analysis is another important tool used in the determination of the surface morphology of an adsorbent. In this study, SEM was used to probe the change in morphological features of nano I-S_m and Pb-adsorbed nano I-S_m (Figure 2).

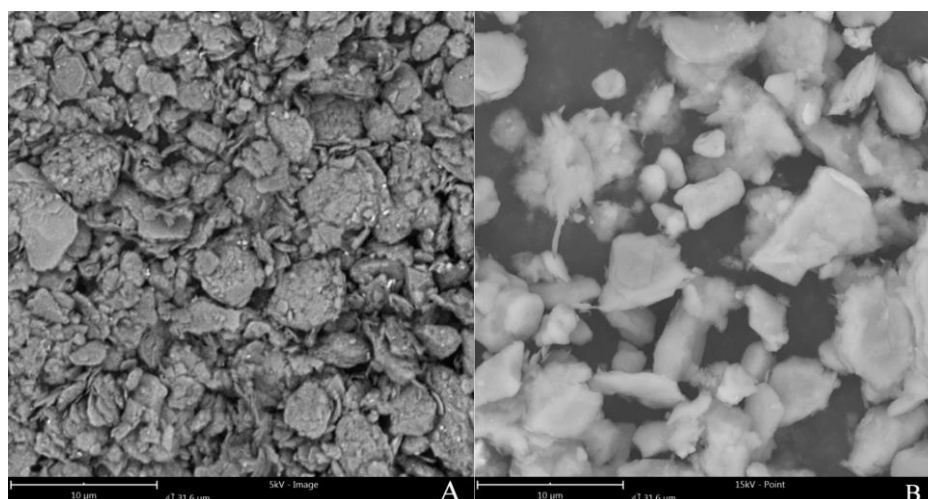


Figure 2. (A) SEM micrograph of nano I-S_m (before adsorption); (B) after Pb(II) adsorption.

3.2. Effect of Adsorption Conditions

3.2.1. Effect of pH

The effect of pH on Pb(II) removal rate was investigated at 298 K for 60 min as shown in Figure 3A. It was observed that the levels of adsorption efficiency of Pb(II) increased significantly with increasing pH. The removal rate of Pb(II) on nano I-S_m was only 41.25 % at pH 2.0. In addition, the removal rate of Pb(II) tended to equilibrate at pH 4.0. When the solution had a pH > 6.0, the solution of Pb(II) gradually formed Pb(OH)₂ precipitate, and the solution system became relatively complex.

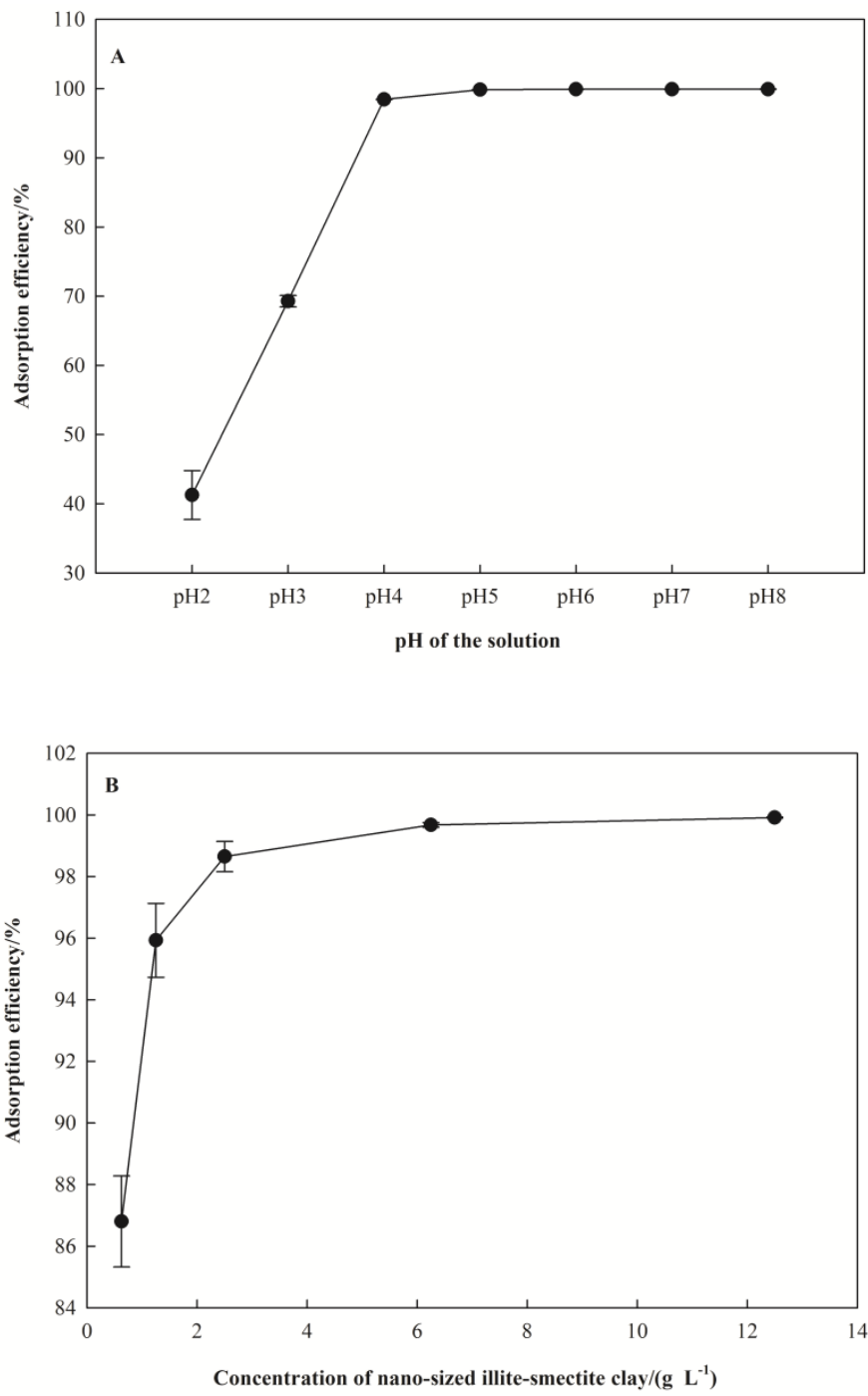


Figure 3. Cont.

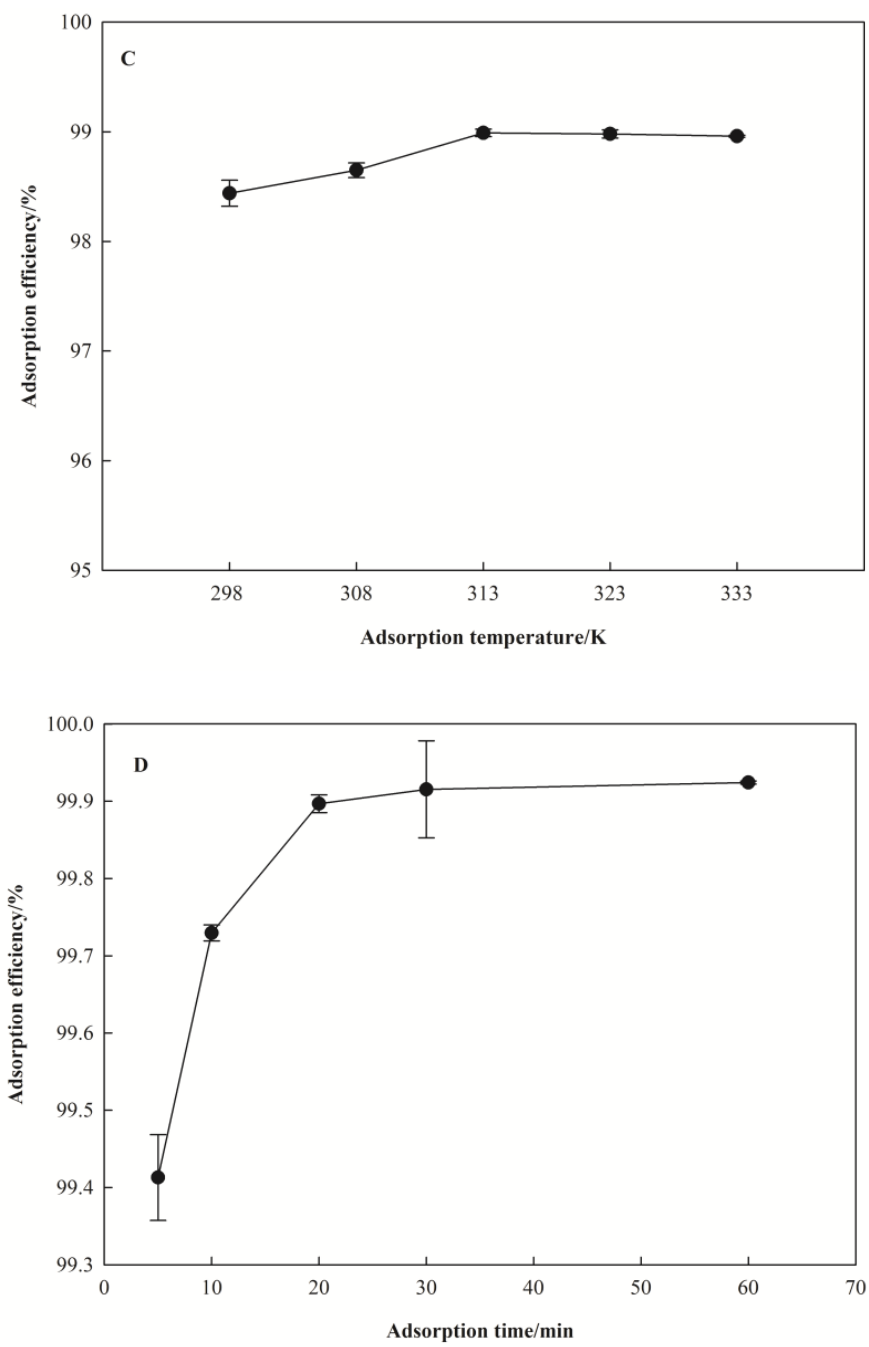


Figure 3. Cont.

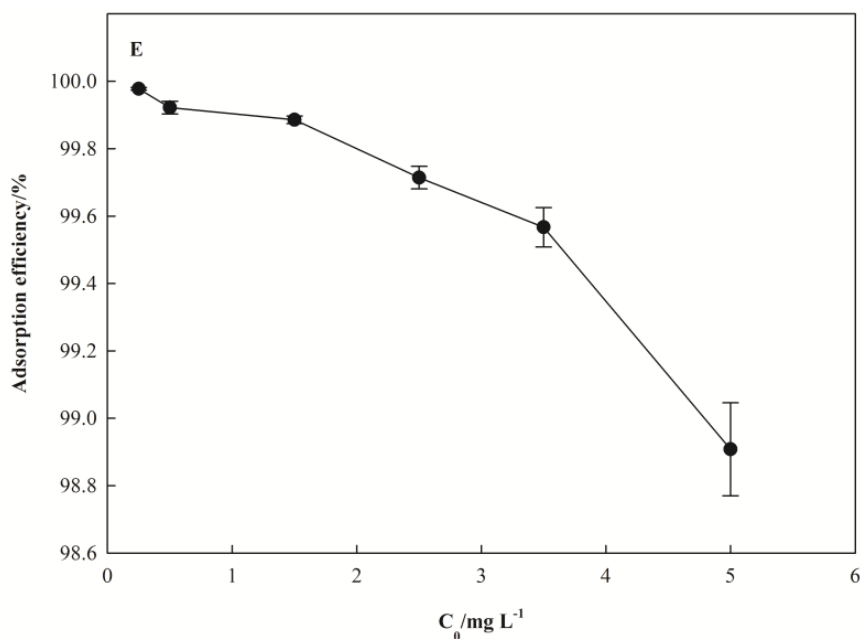


Figure 3. Effect of adsorption conditions on the removal rate of Pb(II). (A) for pH, (B) for dosage of I-S_m, (C) for adsorption temperature, (D) for adsorption time, (E) for Pb(II) initial concentration.

3.2.2. Effect of Nano I-S_m Dosage

The effect of nano I-S_m dosage on Pb(II) removal rate is shown in Figure 3B. The nano I-S_m dosage varied from 0.625 to 12.5 g·L⁻¹ with a constant initial Pb(II) concentration of 1 mg·L⁻¹ for 60 min at 298 K. Figure 3B shows the effect of nano I-S_m dosage on the removal rate of Pb(II). It was observed that the removal rate of Pb(II) increased with an increase in the nano I-S_m dosage from 0.625 to 2.5 g·L⁻¹. A further increase in the nano I-S_m dosage, however, did not result in a sufficient increase in the removal rate of Pb(II).

3.2.3. Effect of Adsorption Temperature

The effect of temperature on Pb(II) removal rate is shown in Figure 3C. It was observed that the removal rate of Pb(II) was 98.44–98.99% when the temperature was set at 298, 308, 313, 323, and 333 K. The trend of the removal rate with the increase of temperature is not obvious.

3.2.4. Effect of Adsorption Time

The effect of adsorption time on the removal rate of Pb(II) is shown in Figure 3D. In a Pb(II) solution with a low initial concentration, the removal rate of Pb(II) in solution reached 99.41% when the adsorption time was 5 min, and the removal rate of Pb(II) tended to be stable after 20 min.

3.2.5. Effect of Initial Concentration of Pb(II)

The effect of initial concentration on the removal rate of Pb(II) adsorbed by nano I-S_m is shown in Figure 3E. The removal rate of Pb(II) decreased with the increase of initial Pb(II) concentration. When the initial concentration of Pb(II) increased from 0.25 to 5 mg·L⁻¹, the removal rate of Pb(II) decreased from 99.45% to 98.90%.

3.3. Kinetic Parameters of the Adsorption

The kinetic of adsorption of Pb(II) on nano I-S_m was fitted by pseudo-first-order and pseudo-second-order kinetic equations. The results are shown in Table 2 and Figure 4. The correlation coefficient of the linear plots of t/Q_t against t for the pseudo-first-order model and the pseudo-second-order

model was 0.985 and 1, respectively. The Q_e of the pseudo-first-order kinetics model was $2.603 \mu\text{g}\cdot\text{g}^{-1}$, and the Q_e of pseudo-second-order dynamic model was $256.410 \mu\text{g}\cdot\text{g}^{-1}$.

Table 2. The predicted parameters by pseudo-first-order and pseudo-second-order kinetic models and experimental data.

Pseudo-First-Order Kinetic Model			Pseudo-Second-Order Kinetic Model			Experimental Data
k_1/min^{-1}	$Q_e/(\mu\text{g}\cdot\text{g}^{-1})$	R^2	$K_2/(\mu\text{g}\cdot\text{g}^{-1}\cdot\text{min}^{-1})$	$Q_e/(\mu\text{g}\cdot\text{g}^{-1})$	R^2	$Q_e/(\mu\text{g}\cdot\text{g}^{-1})$
0.380	2.603	0.985	0.251	256.410	1.000	254.680

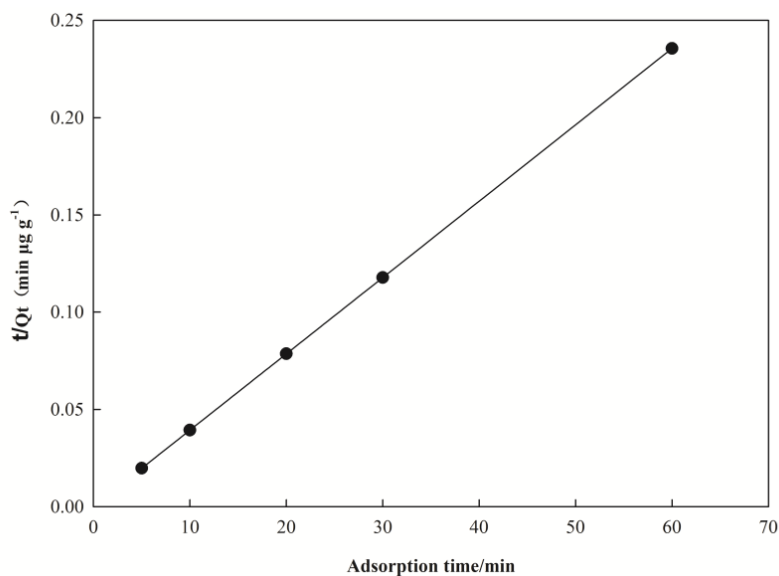


Figure 4. Pseudo-second-order plots for the adsorption of Pb(II) at 298 K.

3.4. Equilibrium Parameters of the Adsorption

The Langmuir and Freundlich isotherm models were used to analyze the adsorption of Pb(II) on nano I-S_m. All of the isotherm constants and correlation coefficients were calculated from the linear forms of the isotherm model equations and are provided in Table 3 and Figure 5.

Table 3. Parameters calculated by the Langmuir and Freundlich isotherm models for the adsorption of Pb(II) on nano I-S_m.

Langmuir			Freundlich		
$Q_{\max}/(\text{mg}\cdot\text{g}^{-1})$	$K_L/(\text{L}\cdot\mu\text{g}^{-1})$	R^2	$K_f/(\mu\text{g}\cdot\text{g}^{-1})$	$1/n$	R^2
2.104	0.216	0.985	8.825	0.457	0.980

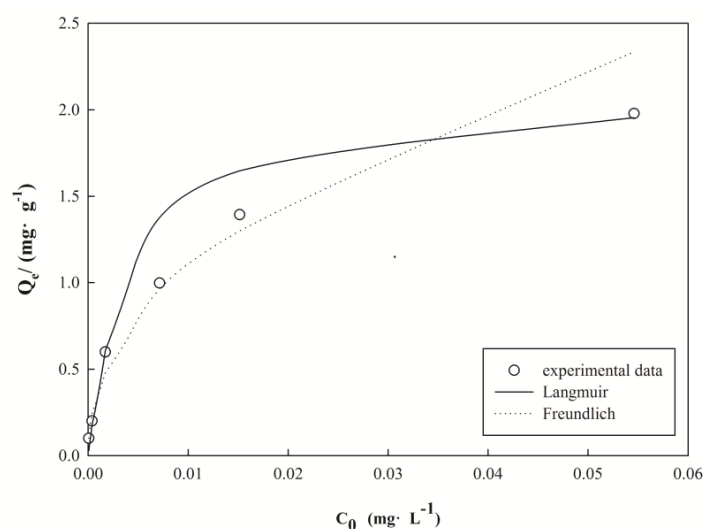


Figure 5. Comparison of equilibrium isotherms between the experimental data and the theoretical data.

3.5. Thermodynamic Parameters of the Adsorption

The results of the analysis of the thermodynamic parameters of adsorption are shown in Table 4 and Figure 6.

Table 4. Thermodynamic parameters for adsorption of Pb^{2+} on nano I-S_m.

ΔS	ΔH	$\Delta G/(\text{kJ}\cdot\text{mol}^{-1})$				
		298 K	308 K	313 K	323 K	333 K
$\text{J}\cdot\text{mol}^{-1}\cdot\text{K}^{-1}$	$\text{kJ}\cdot\text{mol}^{-1}$	298 K	308 K	313 K	323 K	333 K
9.658	4.844	−2.541	−2.637	−2.695	−2.788	−2.876

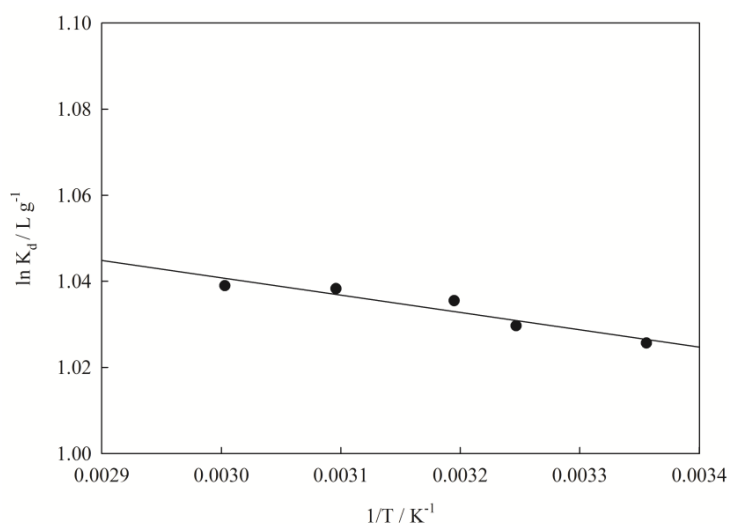


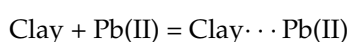
Figure 6. Relationship between $1/T$ and $\ln K_d$ for nano I-S_m.

4. Discussion

Among the adsorption conditions, the pH of the aqueous solution is an important variable for the adsorption of metals onto the adsorbents [32]. In this study, the adsorption efficiency was significantly inhibited when the pH of the aqueous solution was low. At a low pH, the number of H^+ ions exceeds that of $\text{Pb}(\text{II})$ ions several times and the surface of nano I-S_m is most likely covered with H^+ ions,

which account for less Pb(II) adsorbed [33]. As the pH increases, more and more H^+ ions leave the nano I-S_m surface, making the sites available to the Pb(II), which could increasingly bind to the nano I-S_m surface through a mechanism similar to that of exchange interactions (H(I)/Pb(II)) [28]. In the meantime, Yuan et al. [19] have found that the Zeta potential decreased from 3.29 to -69.95 mV when the pH value increased from 2 to 7 in a nano I-S_m solution, indicating that the surface charge of the nano I-S_m changed from positive to negative, and further verifying the deprotonation processes of nano- I-S_m with the increase of pH. It was observed that nano I-S_m was suitable for removing Pb(II) from waste water under an acidic condition, which was similar to the results of some clay adsorbing heavy metals [28,29]. The removal rate of Pb(II) is also related to the I-S_m dosage. At a lower nano I-S_m dosage, Pb(II) ions compete for the limited adsorption sites in the nano I-S_m. As the quantity of nano I-S_m increased, more available sites promoted a greater percentage removal of Pb(II) [33]. When the amount of nano I-S_m was $6\text{ g}\cdot\text{L}^{-1}$, $1\text{ mg}\cdot\text{L}^{-1}$ Pb(II) in solution would be reduced to $0.01\text{ mg}\cdot\text{L}^{-1}$, reaching the potable water standard. In addition, nano I-S_m showed a rapid adsorption effect in the temperature range of 298–333 K. The above results revealed an important advantage of high efficiency removal of Pb(II) by the nano I-S_m.

The Q_e of the pseudo-second-order dynamic model was much closer to the experimental result and the correlation coefficients were found to be relatively high. The pseudo-second-order adsorption mechanism was predominant for the adsorption of Pb(II) on nano I-S_m. The pseudo-second-order model assumes that two reactions are happening: the first one is fast and reaches equilibrium quickly, whereas the second one is a slower reaction [15]. Accordingly, the following mechanism may be proposed [33]:



in which the number of adsorption sites on the nano I-S_m surface and the number of Pb(II) ions in the liquid phase determine the kinetics. Depending on pH, different Pb-species may be held to the clay surface at appropriate ion-exchange sites [25,33].

The correlation coefficient of the Langmuir isotherm model was higher than that of the Freundlich isothermal model, from which we can conclude that the Langmuir isotherm model was more suitable for nano I-S_m removal of Pb(II) in aqueous solutions. Similar results were also reported in earlier studies in which the adsorption of heavy metal ions fitted well to the Langmuir isotherm [15,19,33]. Furthermore, the n values of the Freundlich isothermal model relate to the adsorption properties of the adsorbent, where values of n between 2 and 10 represent good adsorption [34], which is an indication of the good adsorption of Pb(II) by nano I-S_m.

The Gibbs free energy (ΔG) was -2.541 , -2.637 , -2.695 , -2.788 , and $-2.876\text{ kJ mol}^{-1}$ ($\Delta G < 0$) when the temperature was set at 298, 308, 313, 323, and 333 K, respectively. These indicate that the adsorption of Pb(II) on nano I-S_m is a spontaneous process [23]. The ΔH was 4.844 kJ mol^{-1} ($0 < \Delta H < 16$), which indicates that the adsorption of Pb(II) on nano I-S_m is an endothermic process [19,34].

The SEM results showed that the surface morphology of Pb-adsorbed nano I-S_m is different from that of natural nano I-S_m. The natural nano I-S_m showed loose aggregates with a porous structure. After adsorption, the surface of nano I-S_m demonstrates compacted aggregates. The surface morphology of the natural nano I-S_m changed evidently during the adsorption process, indicating that significant interaction at the lead–clay interface occurred during the experiment. Similar SEM results were reported by other researchers [28,35].

5. Conclusions

As a new adsorbent, nano I-S_m can be used for depth treatment in lead-contaminated water. The pseudo-second-order adsorption mechanism was predominant for the adsorption of Pb(II) on nano I-S_m. The saturated adsorption capacity of Pb(II) on nano I-S_m in the aqueous solution was $256.41\text{ }\mu\text{g}\cdot\text{g}^{-1}$. The adsorption patterns followed the Langmuir isotherm model. The adsorption of Pb(II) on nano I-S_m is a thermodynamically feasible, spontaneous, and endothermic process.

Acknowledgments: This work was supported by the Guangxi Natural Science Foundation (grant No. 2015GXNSFEA139001) from the Guangxi science and Technology Department, the project of International Scientific Exchange Program (grant No. 7–1, 2017) from the Ministry of Science and Technology of the People’s Republic of China, and the key project of Guangxi Social Sciences. (grant No. gxsk201605)

Author Contributions: Juan Yin and Chaobing Deng designed the study; Juan Yin and Zhen Yu analyzed the data; Juan Yin wrote the article, and Xiaofei Wang and Guiping Xu provided access to the experimental site.

Conflicts of Interest: The authors declare no conflict of interest.

References

1. Dipak, P. Research on heavy metal pollution of river Ganga: A review. *Ann. Agrar. Sci.* **2017**, *15*, 278–286. [[CrossRef](#)]
2. IslamabMd, M.S.; Ahmed, M.K.; Raknuzzaman, M.; Mamun, M.H.-A.; Islam, M.K. Heavy metal pollution in surface water and sediment: A preliminary assessment of an urban river in a developing country. *Ecol. Indic.* **2015**, *48*, 282–291. [[CrossRef](#)]
3. Xie, X.J.; Wang, F.Y.; Wang, G.J.; Mei, R.W.; Wang, C.Z. Study on Heavy Metal Pollution in Surface Water in China. *Environ. Sci. Manag.* **2017**, *42*, 31–34. [[CrossRef](#)]
4. Zhang, X.W.; Yang, L.S.; Li, Y.H.; Li, H.R.; Wang, W.Y.; Ye, B.X. Impacts of lead /zinc mining and smelting on the environment and human health in China. *Environ. Monit. Assess.* **2012**, *184*, 2261–2273. [[CrossRef](#)] [[PubMed](#)]
5. Li, Z.Y.; Ma, Z.W.; Kuijp, T.J.; Yuan, Z.W.; Huang, L. A review of soil heavy metal pollution from mines in China: Pollution and health risk assessment. *Sci. Total Environ.* **2014**, *468–469*, 843–853. [[CrossRef](#)] [[PubMed](#)]
6. Ahmaruzzaman, M.; Gupta, V.K. Rice husk and its ash as low-cost adsorbents in water and wastewater treatment. *Ind. Eng. Chem. Res.* **2011**, *50*, 13589–13613. [[CrossRef](#)]
7. Zhao, D.D.; Yu, Y.; Chen, P. Treatment of lead contaminated water by a PVDF membrane that is modified by zirconium, phosphate and PVA. *Water Res.* **2016**, *101*, 564–573. [[CrossRef](#)] [[PubMed](#)]
8. Vergili, I.; Gönder, Z.B.; Kaya, Y.; Gürdağ, G.; Çavuş, S. Sorption of Pb (II) from battery industry wastewater using a weak acid cation exchange resin. *Process Saf. Environ. Prot.* **2017**, *107*, 498–507. [[CrossRef](#)]
9. Milind, M.N.; Santosh, K.D. Lead resistant bacteria: Lead resistance mechanisms, their applications in lead bioremediation and biomonitoring. *Ecotox. Environ. Saf.* **2013**, *98*, 1–7. [[CrossRef](#)]
10. Abreham, T.B.; Abaynesh, Y.G.; Ramato, A.T.; Dawit, N.; Efreem, C.; Lidietta, G. Removal of emerging micropollutants by activated sludge process and membrane bioreactors and the effects of micropollutants on membrane fouling: A review. *J. Environ. Chem. Eng.* **2017**, *5*, 2395–2414. [[CrossRef](#)]
11. Zhao, G.X.; Li, J.X.; Ren, X.M.; Chen, C.L.; Wang, X.K. Few-layered graphene oxide nanosheets as superior sorbents for heavy metal ion pollution management. *Environ. Sci. Technol.* **2011**, *45*, 10454–10462. [[CrossRef](#)] [[PubMed](#)]
12. Burakov, A.E.; Galunin, E.V.; Burakova, I.V.; Kucherova, A.E.; Agarwal, S.; Tkachev, A.G.; Gupta, V.K. Adsorption of heavy metals on conventional and nanostructured materials for wastewater treatment purposes: A review. *Ecotoxicol. Environ. Saf.* **2018**, *148*, 702–712. [[CrossRef](#)] [[PubMed](#)]
13. Mohammad, K.U. A review on the adsorption of heavy metals by clay minerals, with special focus on the past decade. *Chem. Eng. J.* **2017**, *308*, 438–462. [[CrossRef](#)]
14. Masindi, V.; Gitari, W.M. Simultaneous removal of metal species from acidic aqueous solutions using cryptocrystalline magnesite/bentonite clay composite: An experimental and modelling approach. *J. Clean. Prod.* **2016**, *112*, 1077–1085. [[CrossRef](#)]
15. Joziane, G.M.; Murilo, P.M.; Thirugnanasambandham, K.; Sergio, H.B.F.; Marcelino, L.G.; Maria, A.S.D.B.; Sivakumar, V. Preparation and characterization of calcium treated bentonite clay and its application for the removal of lead and cadmium ions: Adsorption and thermodynamic modeling. *Process Saf. Environ.* **2017**, *111*, 244–252. [[CrossRef](#)]
16. Sari, A.; Tuzen, M. Cd(II) adsorption from aqueous solution by raw and modified kaolinite. *Appl. Clay Sci.* **2014**, *88–89*, 63–72. [[CrossRef](#)]
17. Atta, A.M.; Al-Lohedan, H.A.; AlOthman, Z.A.; Abdel-Khalek, A.A.; Tawfeek, A.M. Characterization of reactive amphiphilic montmorillonite nanogels and its application for removal of toxic cationic dye and heavy metals water pollutants. *J. Ind. Eng. Chem.* **2015**, *31*, 374–384. [[CrossRef](#)]

18. Qiu, J.Y. Preparation of Illite/Smectite Clay Nano-Powder and Its Application as Rubber Filler. Master's Thesis, South China University of Technology, Guangzhou, China, 4 June 2014.
19. Yuan, S.S.; Li, Z.Y.; Pan, Z.D.; Wang, Y.M. Removal of Copper and Cadmium Ions in Aqueous Solution via Adsorption by Nano-sized Illite-Smectite Clay. *J. Chin. Ceram. Soc.* **2016**, *44*, 43–49. [[CrossRef](#)]
20. Zhang, L.H.; Yuan, Y.H.; Yan, Z.G.; Zhou, Y.Y.; Zhang, C.Y.; Huang, Y.; Xu, M. Application of nano illite/smectite clay for adsorptive removal of metals in water. *Res. Environ. Sci.* **2016**, *29*, 115–123. [[CrossRef](#)]
21. Sakthivel, S.; Venkatesan, V.; Krishnan, B.; Pitchumani, B. Influence of suspension stability on wet grinding for production of mineral nanoparticles. *Particuology* **2008**, *6*, 120–124. [[CrossRef](#)]
22. Bao, S.D. *Soil Agricultural Chemistry Analysis*, 3rd ed.; China Agricultural Press: Beijing, China, 2000; pp. 152–176, ISBN 9787109066441.
23. Dawodu, F.A.; Akpomie, K.G. Simultaneous adsorption of Ni(II) and Mn(II) ions from aqueous solution onto a Nigerian kaolinite. *J. Mater. Res. Technol.* **2014**, *3*, 129–141. [[CrossRef](#)]
24. Lagergren, S. *Zur theorie der sogenannten adsorption gelöster stoffe (about the theory of so-called adsorption of soluble substances)*; Kungliga Svenska Vetenskapsakademiens (Royal Swedish Academy of Sciences): Stockholm, Sweden, 1898; pp. 1–39.
25. Ho, Y.S.; McKay, G. Pseudo-second order model for sorption processes. *Process Biochem.* **1999**, *34*, 451–465. [[CrossRef](#)]
26. Langmuir, I. The adsorption of gases on plane surfaces of glass, mica and platinum. *J. Am. Chem. Soc.* **1918**, *40*, 1361–1403. [[CrossRef](#)]
27. Freundlich, H.M.F. Über die adsorption in lösungen. *Z. Phys. Chem.* **1906**, *57*, 385–470. [[CrossRef](#)]
28. Jiang, M.Q.; Wang, Q.P.; Jin, X.Y.; Chen, Z.L. Removal of Pb(II) from aqueous solution using modified and unmodified kaolinite clay. *J. Hazard. Mater.* **2009**, *170*, 332–339. [[CrossRef](#)] [[PubMed](#)]
29. Olgun, A.; Atar, N. Equilibrium, thermodynamic and kinetic studies for the adsorption of lead (II) and nickel (II) onto clay mixture containing boron impurity. *J. Ind. Eng. Chem.* **2012**, *18*, 1751–1757. [[CrossRef](#)]
30. Campo, M.D.; Bauluz, B.; Nieto, F.; Papa, C.D.; Hongn, F. SEM and TEM evidence of mixed-layer illite-smectite formed by dissolution- crystallization processes in continental Paleogene sequences in northwestern Argentina. *Clay Miner.* **2016**, *51*, 723–740. [[CrossRef](#)]
31. Li, Y.J.; Zeng, L.; Zhou, Y.; Wang, T.F.; Zhang, Y.J. Preparation and Characterization of Montmorillonite Intercalation Compounds with Quaternary Ammonium Surfactant: Adsorption Effect of Zearalenone. *J. Nanomater.* **2014**, 2014. [[CrossRef](#)]
32. Deng, L.L.; Yuan, P.; Liu, D.; Liu, Z.W. Effects of microstructure of clay minerals, montmorillonite, kaolinite and halloysite, on their benzene adsorption behaviors. *Appl. Clay Sci.* **2017**, *143*, 184–191. [[CrossRef](#)]
33. Krishna, G.B.; Susmita, S.G. Pb(II) uptake by kaolinite and montmorillonite in aqueous medium: Influence of acid activation of the clays. *Colloid Surf. A* **2006**, *277*, 191–200. [[CrossRef](#)]
34. Nir, S.; Undabeytia, T.; Dana, Y.; Yasser, E.; Polubesova, T.; Serban, C.; Rytwo, G.; Lagaly, G.; Rubin, B. Optimization of adsorption of hydrophobic herbicides on montmorillonite presorbed by monovalent organic cations: Interaction between phenyl rings. *Environ. Sci. Technol.* **2000**, *34*, 1269–1274. [[CrossRef](#)]
35. Li, J.S.; Xue, Q.; Wang, P.; Li, Z.Z. Effect of lead (II) on the mechanical behavior and microstructure development of a Chinese clay. *Appl. Clay Sci.* **2015**, *105–106*, 192–199. [[CrossRef](#)]

